THE UNIVERSITY of EDINBURGH

Edinburgh Research Explorer

Understanding Hysteresis and Gas Trapping in Dissociating Hydrate-Bearing Sediments Using Pore Network Modeling and Three-Dimensional Imaging

Citation for published version:
Li, M, Jian, Z, Hassanpouryouzband, A & Zhang, L 2022, 'Understanding Hysteresis and Gas Trapping in Dissociating Hydrate-Bearing Sediments Using Pore Network Modeling and Three-Dimensional Imaging', *Energy and Fuels*, vol. 36, no. 18, pp. 10572-10582. https://doi.org/10.1021/acs.energyfuels.2c01306

Digital Object Identifier (DOI):
10.1021/acs.energyfuels.2c01306

Link:
Link to publication record in Edinburgh Research Explorer

Document Version:
Publisher's PDF, also known as Version of record

Published In:
Energy and Fuels

General rights
Copyright for the publications made accessible via the Edinburgh Research Explorer is retained by the author(s) and / or other copyright owners and it is a condition of accessing these publications that users recognise and abide by the legal requirements associated with these rights.

Take down policy
The University of Edinburgh has made every reasonable effort to ensure that Edinburgh Research Explorer content complies with UK legislation. If you believe that the public display of this file breaches copyright please contact openaccess@ed.ac.uk providing details, and we will remove access to the work immediately and investigate your claim.

Download date: 21. Sep. 2023

energy&fuels

pubs.acs.org/EF

Article

Understanding Hysteresis and Gas Trapping in Dissociating Hydrate-Bearing Sediments Using Pore Network Modeling and Three-Dimensional Imaging

Min Li, Zhenhe Jian, Aliakbar Hassanpouryouzband,* and Lunxiang Zhang*

Cite This: *Energy Fuels* 2022, 36, 10572−10582

Read Online

ACCESS | Metrics & More | Article Recommendations | Supporting Information

ABSTRACT: Hysteresis behavior is a key factor in exploring dynamic water and gas flow in dissociating hydrate-bearing sediments (HBS). In this study, we combined microfocus X-ray computed tomography and a pore network model to investigate the effect of hydrate dissociation on gas trapping and hysteresis in capillary pressure, P_c and relative permeability, k_r in different wettability systems. The results show that the hydrate dissociation process involves secondary hydrate formation, which promotes gas trapping. The effective residual gas saturation in the water-wet system was significantly higher than that in the gas-wet system due to snap-off. Gas trapping has a huge impact on the hysteresis in P_c and k_r between the drying and wetting cycles in HBS. This work will improve the fundamental understanding of the permeability properties of HBS so that gas and water production can be better assessed.

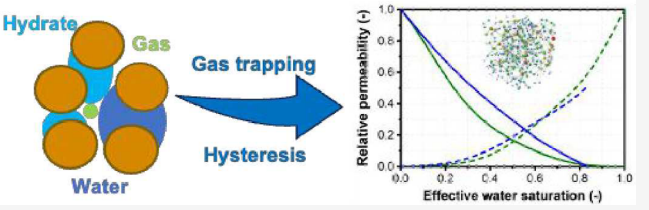

1. INTRODUCTION

Gas hydrates are a type of icelike crystalline compound that form under preferably low temperature and elevated pressure,[1] where water molecules form cagelike structures that trap "guest" molecules like methane and carbon dioxide.[2] The amount of methane stored in gas hydrates along continental shelf and slope regions, permafrost areas, and inland seas is estimated to be at least twice that of conventional hydrocarbon sources.[3,4] Gas hydrates can decompose and release the stored guest gas molecules if the temperature or pressure falls outside the hydrate stability zone. Accordingly, different methods have been proposed to extract methane from these low-carbon energy reservoirs. The process of extracting natural gas from hydrate-bearing sediments (HBS) is described as a multiphase flow associated with chemical reactions within a porous medium, involving heat transfer,[5] water and gas flow,[6,7] fine-particle migration,[8] and hydrate phase transition.[9,10] To characterize multiphase flow properties in HBS, permeability measurement is needed, which is critical to understanding water and gas production[11,12] and methane releases from hydrates into the atmosphere and ocean.[13]

Hydrates occupy the pore space in HBS and influence the effective permeability, k_{eff} (i.e., single-phase permeability), which is defined as the intrinsic (or absolute) permeability, k_{int}, that reflects the intrinsic ability of sediments without hydrates to allow single-phase flow and does not depend on the fluid type.[11,14] In two-phase fluid systems, the competitive flow is described by the relative permeability, k_r. The permeability of HBS is affected by many factors, such as hydrate saturation and distribution,[12,15] sediment wettability,[16] and rock and fluid properties. Sediment rocks usually contain quartz, feldspars, calcite, and clay with different contact angles, where fluid flow is usually accompanied with wettability alteration.[17] Extensive experimental studies[18−20] as well as continuously improved pressure core technologies and downhole techniques[21,22] have yielded reliable permeability. However, these methods are not ideal for permeability measurement and still undergo secondary hydrate formation, changes in hydrate morphology, and evolutions in the pore structure.

Many researchers pay more attention to the effect of hydrate saturation, S_h and pore habit on permeability through laboratory experiments.[8,18,19,21] The experimental results have confirmed that the hydrates occurred in the pore space and reduced the pore size and hindered the water and gas flow. The permeability is difficult to measure because the primary challenge is the thermodynamic instability of gas hydrates in HBS.[23] A recent study[14] reported that the unsteady-state permeability method was a reliable and reproducible way for fluid flow measurement, which is a faster method of permeability testing in HBS. It requires effectively controlled independent pore, radial, and axial pressure, accurate specimen and surroundings temperature, necessarily injecting front-end saturation skills, and precise experimental processes. Moreover,

Special Issue: 2022 Pioneers in Energy Research: John Ripmeester

Received: April 26, 2022
Revised: July 16, 2022
Published: August 4, 2022

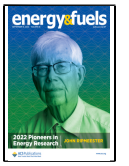

Downloaded via UNIV OF EDINBURGH on September 12, 2023 at 16:07:56 (UTC).
See https://pubs.acs.org/sharingguidelines for options on how to legitimately share published articles.

© 2022 The Authors. Published by American Chemical Society

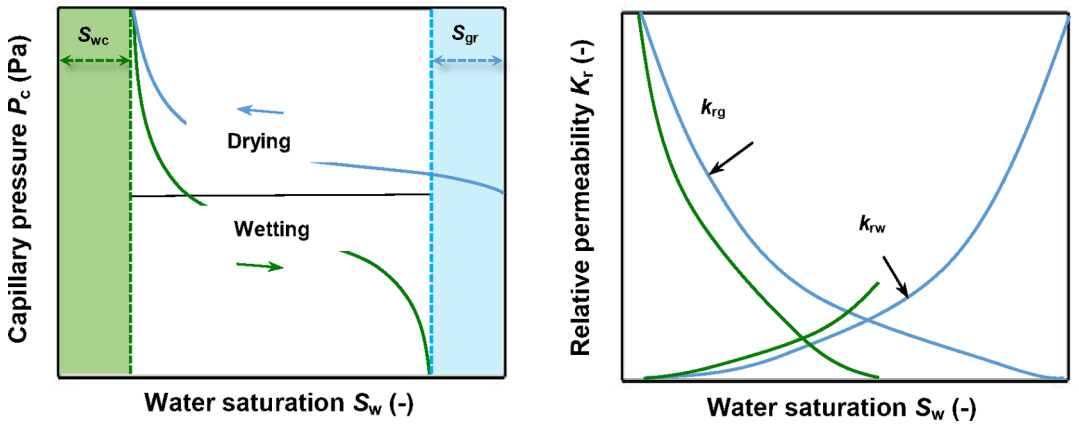

Figure 1. Schematic diagram of the hysteresis in P_c and k_r.

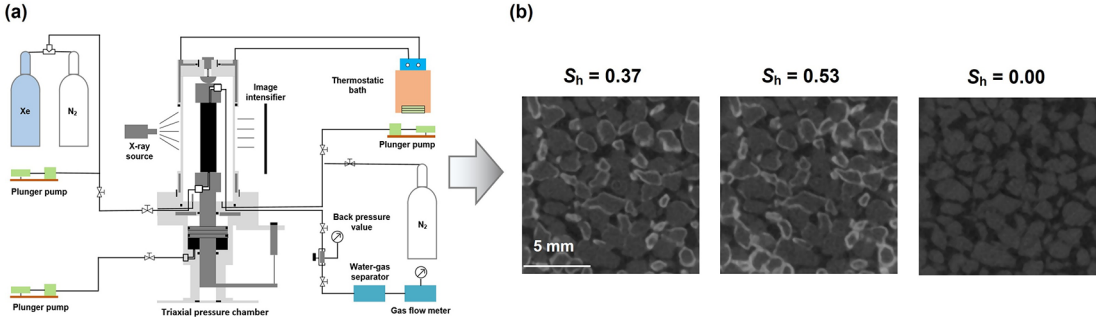

Figure 2. (a) Schematic diagram of a triaxial testing apparatus and micrometer-resolution X-ray CT (ref 49). (Reprinted with permission from ref 49. Copyright 2021 American Chemical society.) (b) Cross section of CT images of the hydrate dissociation process.

experimental challenges have led researchers to pay more attention to the prediction of water relative permeability, k_{rw}, and gas relative permeability, k_{rg}, using theoretical analysis and numerical methods; however, these results still lack verification via experimental results.

In recent years, many theoretical analyses[24,25] and numerical simulation methods have been used to study the permeability of HBS: especially the lattice Boltzmann method[26] and pore network model (PNM).[27] The PNM is an efficient method for analyzing the permeability, which is based on microfocus X-ray computed tomography (CT) that directs imaging of pore structures and fluid distributions in a different porous medium.[8,16,28−30] Extensive PNM studies[31−33] have been developed for analyzing CT images, and these simulation methods have been applied in environmental engineering,[34] groundwater hydrology,[35] and petroleum engineering.[36] PNM can provide the pore space characteristic parameters of HBS,[9] which are used as inputs to predict fluid transport properties by employing the capillary pressure, P_c and k_r curves.[27,37] Wang et al. investigated the effect of particle size, wettability, and surface tension on P_c and k_r using a PNM.[16,27,38]

The P_c and k_r curves generally exhibit a hysteresis phenomenon between drying (drainage) and wetting (imbibition) cycles,[39−42] as shown in Figure 1. These cycles can describe the fluid flow when the water saturation, S_w, gradually decreases and increases in a porous medium.[43] The transition between the drying and wetting cycles is called scanning flow.[44,45] Gas and water production from HBS is a complex multiphase flow process that can also present drying and wetting cycles.[11,21] Hydrate dissociation generates free gas, which is dominated by the drying cycle.[11] The three main types of wetting-dominant ones include (1) water production, which increases the pore water pressure,[11] (2) fluid (e.g., hot water) injection in sediments,[46] and (3) secondary hydrate formation that consumes a large amount of gas and decreases the local gas pressure and P_c.[47] Few studies have been conducted to explore the hysteresis phenomenon in HBS using both experimental[46] and numerical methods.[11] Nevertheless, the understanding of hysteresis in HBS is still unclear; hence, it is important to investigate the effect of hysteresis on water and gas flow in HBS (Figure 1).

As the overall aim of this study, we integrated pore-scale modeling with three-dimensional (3D) imaging to determine the missing parameters for establishing gas recovery from HBS. We combined an *in situ* microfocus X-ray CT observation and a PNM simulation to explore the hysteresis behavior in dissociating HBS. The feasibility and accuracy of PNM in HBS were validated by Wang et al.[27] We extracted equivalent pore networks with parametrized characteristics from 3D images. First, the influence of wettability (water-wet or gas-wet) and pore structure changes during hydrate dissociation on gas trapping were investigated, and the effect of gas trapping on the hysteresis in P_c and k_r between the drying and wetting cycles was analyzed. Moreover, we used dynamic scanning flow to predict complex water and gas displacement sequences in the dissociating HBS.

2. METHODOLOGY

2.1. Experimental Apparatus and Materials. The experimental system consisted of a triaxial testing apparatus and micrometer-resolution X-ray CT (SMX225CTS-SV, Shimadzu Co., Japan), as shown in Figure 2a, and has been thoroughly described by Wu et al.[48]

https://doi.org/10.1021/acs.energyfuels.2c01306
Energy Fuels 2022, 36, 10572−10582

The triaxial testing apparatus included three plunge pumps (GDS Instruments Co., U.K.), a thermostatic bath (FP50-ME, Julabo Co., Germany), a back pressure (KPB-IN0D422P200 K0, Swagelok., U.S.A.) valve, a triaxial pressure chamber, a displacement transducer, and corresponding gas sources. The plunge pumps controlled the pore pressure, axial stress, and confining pressure. A thermostatic bath controlled the temperature with a precision of ±0.01 °C. The back pressure valve controlled the pressure with a precision of ±0.1 MPa.

Fujian sand (Isosand Co., China) which has a density of 2.41 g/cm^3, particle size of 1.33 mm, and a uniformity coefficient of 2.23 was chosen as the host sediment. Xenon and water were used to form xenon hydrate in sand sediments. Xenon has been widely used as a substitute for methane for *in situ* CT experimental studies to enhance the density contrast differences between different phases.[50] In addition to the similar solubilities and diffusivities of xenon gas and methane gas, xenon hydrates and methane hydrates have similar physical properties.[50] Moreover, the experimental conditions required for formation of xenon hydrates are relatively milder than those for methane hydrates, which reduces the potential danger of explosive gas operation under high pressures.

2.2. Experimental Procedure. For the *in situ* observations, the xenon hydrate formation and dissociation were performed in four stages as follows:

(1) Specimen preparation: Water (1.6 g) was mixed with the dried Fujian sand (18.2 g) in a sealed bag, and the resulting wet sand was loaded into the mold (with a diameter of 20 mm and length of 40 mm) and compacted with a tamper. The initial porosity and initial water saturation were 0.40 and 0.32, respectively. After forming the specimen, it would undergo hydrate formation and hydrate dissociation under a specific temperature and pore pressure (xenon gas), as shown in Figure 3. The mold filled with wet sand was placed in a freezer (−4 °C). The frozen specimen was then removed from the mold and placed on the pedestal of the triaxial pressure chamber (state a). Then, the pressure chamber was filled with the confining fluid (nitrogen gas), and the confining pressure (nitrogen gas) was raised to 0.05 MPa. Next, the temperature of the confining fluid (nitrogen gas) was raised to 18 °C to melt the frozen specimens (state b). Finally, the xenon gas displaced the air in the specimen, and the pore and confining pressures were increased to 0.60 and 0.65 MPa, respectively (state c).

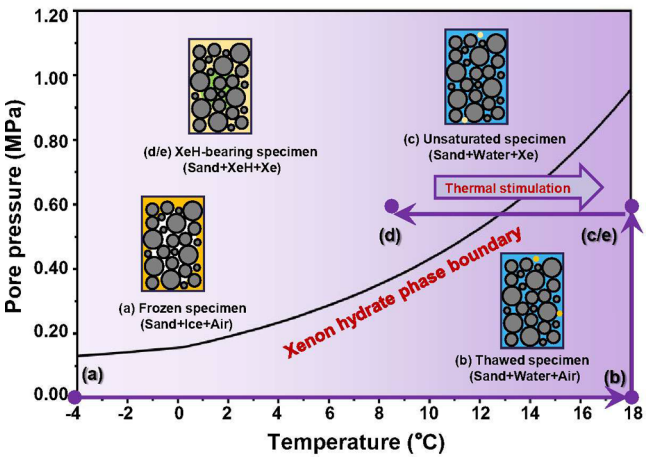

Figure 3. Phase diagram showing the equilibrium conditions for xenon hydrate and the state paths of the pore pressure (xenon gas) and temperature used to produce the xenon hydrate-bearing specimen.

(2) Hydrate formation: To form hydrates, the temperature of the confining fluid was lowered from 18 to 7 °C, and a thermocouple was positioned at the bottom of the specimen to measure the temperature. The confining pressure and pore pressure remained at 0.65 and 0.60 MPa, respectively (state d). When xenon gas consumption was stopped, the hydrates were considered fully formed (all of the water had been converted to hydrates).[48,51,52]

(3) Increase confining pressure: After hydrate formation, the confining pressure was increased from 0.65 to 3.60 MPa to consolidate the specimen.

(4) Hydrate dissociation: Initially, the hydrates were in an equilibrium state with the confining fluid at 7 °C and pore pressure of 0.60 MPa. Then, the temperature of the confining fluid was increased from 7 to 18 °C. The confining pressure and pore pressure remained at 3.60 and 0.60 MPa, respectively (state e). For more details, please refer to previous research.[48]

2.3. CT Image Processing. Micrometer-resolution X-ray CT scans were conducted for the hydrate dissociation process. Each tomogram acquired 1200 projections of the sample over 360° in 320 s. Three groups of original CT images (44 μm/voxel) with 1024 × 1024 × 936 voxel^{3}v (45.06 × 45.06 × 41.18 mm^3) during hydrate dissociation (S_h = 0.37 → S_h = 0.53 → S_h = 0.00) are shown in Figure 2b. The slice data were reconstructed into a 3D volumetric model using InspeXio (Shimadzu Co., Ltd., Japan). Median filtering for noise reduction and watershed segmentation using Fiji (National Institutes for Health, U.S.A.) software were applied to all the original CT images, and then we obtained the binarized images. On the basis of the assumption that the hydrate phase and the sand form the skeleton (the value is 1),[27] the rest of the sample was regarded as the pore space (the value is 0) for extraction of the pore network.

2.4. Representative Elementary Volume Analysis. The representative elementary volume (REV) is a measurement of the minimum volume of a specimen that can represent the characteristic of the whole fluid and sediments.[53,54] This concept commonly uses porosity, ϕ, to define the REV of the specimen as shown in Figure 4.

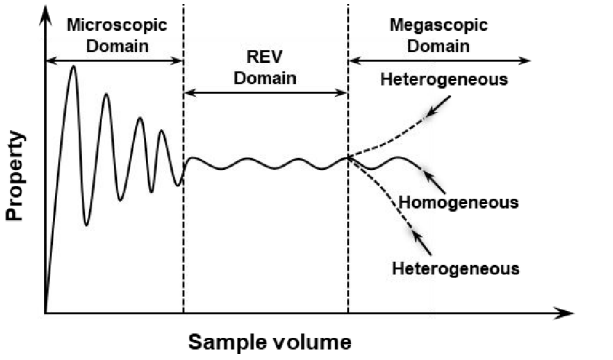

Figure 4. Concept of REV (Adapted with permission from ref 54, Copyright 2015 Springer Verlag.).

In the microscopic domain, the porosity fluctuates unstably with the increase of the sample size. The ϕ fluctuations become insignificant as the sample size is further increased, which means that some properties of the sample become constants that are not affected by the specimen size, which is defined as the REV. In the megascopic domain, the ϕ values may change again as the sample size increases. In this study, a cube of 300 × 300 × 300 voxels^3 (13.20 × 13.20 × 13.20 mm^3) was treated as a REV to extract the 3D pore network (Figure 5). Avizo software is used to visualize the 3D pore network (FEI Hillsboro, U.S.A.).

2.5. Quasi-static Pore Network Modeling. In this work, the open-source code of a PNM was adopted to extract the network from dissociating HBS as shown in Figure 6.[33] By using this method, the uncertainty in conventional network modeling could be reduced. This algorithm calculates a distance map from each pore space voxel to the nearest solid surface. The local maxima on the distance map were defined as pores, and the algorithm was developed using the maximum ball algorithm.[31] The distance map increases on either

https://doi.org/10.1021/acs.energyfuels.2c01306
Energy Fuels 2022, 36, 10572−10582

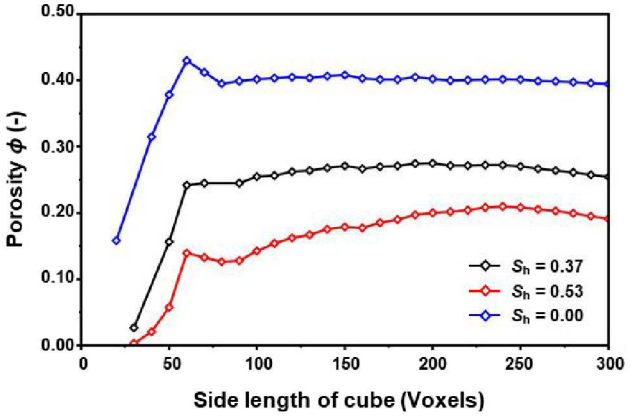

Figure 5. REV analysis for a specimen during the hydrate dissociation process.

side of the pores, defined as throats. More detailed descriptions of this pore and throat determination algorithm have been provided by Raeini et al.[33] The shape factor (G) is used to describe complex and irregular geometrical profiles of the pores and throats. G is defined by Bultreys et al.[55] as follows:

$$G_t = \frac{R^2}{4A} \quad (1)$$

$$G_p = \frac{\sum G_t}{n} \quad (2)$$

where G_p and G_t are the pore shape factor and throat shape factor, respectively; R is the inscribed radius and A is the cross-sectional area; n is the coordination number.

After pore network extraction, water and gas transport in HBS is simulated using a quasi-static invasion percolation approach that is generally performed with a pore network flow simulator.[56] In the simulator, initially, the network is filled with water, which displaces by gas into the largest pores until a very high P_c or target S_w is reached. This process is called drying, where only a single flow pattern occurs: piston-like displacement.[56] After the drying, water displaces the gas in a porous medium until the residual gas saturation S_{gr} is reached; this process is called the wetting process. For HBS, we provided the concept of effective residual gas saturation, S_{ger} (gas trapping), when we simulated the water and gas flow process using the pore network flow simulator. There are three main flow patterns in the pore space: piston-like displacement, pore body filling, and snap-off (Figure S1). As the aspect ratio, r_p, increases, more gas trapping could occur in a porous medium as the result of snap-off.[39,57] The piston-like displacement leads to a relatively flat advance of the fluid, causing a small amount of gas trapping in the pore space. Pore body filling leads to extremely small trapping. Moreover, gas trapping could occur in uninvaded pores and throats,[43] where the gas is surrounded by water layers in the smallest pore space that is unable to escape in the water layer.

The following assumptions are made by the pore network flow simulator: the water phase and the gas phase of the system are incompressible and the viscous force is negligible compared with the capillary force. In addition, gravity is ignored during the simulation process.

2.6. Gas Trapping. Hysteresis in P_c and k_r is primarily caused by trapping and contact angle hysteresis[58] as shown in Figure 7. In the case of a water and gas flow simulation, ignoring hysteresis will produce extremely large errors.[59]

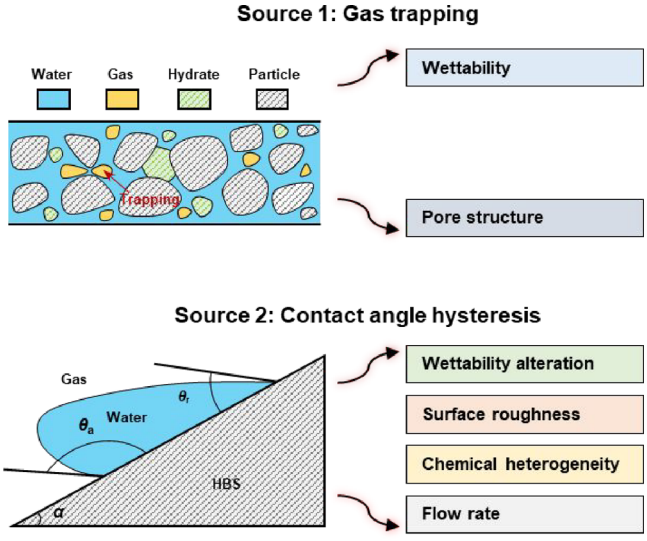

Figure 7. Two main sources for hysteresis in HBS: gas trapping and contact angle hysteresis.

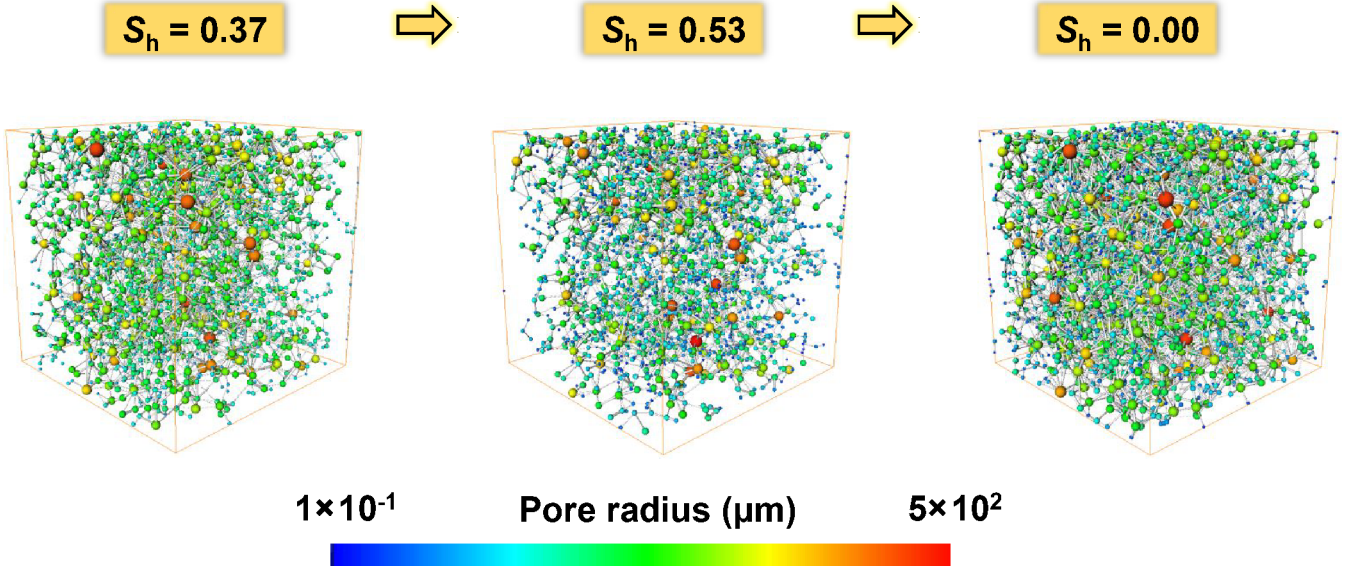

Figure 6. Visualization of pore network models during the hydrate dissociation process.

https://doi.org/10.1021/acs.energyfuels.2c01306
Energy Fuels 2022, 36, 10572−10582

Trapping is a key factor that affects the hysteresis in P_c and k_r in a porous medium.[58] During the wetting cycle, water cannot displace all the gas, and the gas is trapped or stranded by water in the pore space.[43] In principle, trapping is caused by pore structure and wettability. Additionally, contact angle hysteresis influences the hysteresis in P_c and k_r in a porous medium.[58] The contact angle hysteresis is defined as the difference between the receding contact angle θ_r and advancing contact angle θ_a, where θ_r is always smaller than θ_a, as shown in Figure 8. This hysteresis is attributed to wettability alteration, surface roughness, chemical heterogeneity, and flow rate.

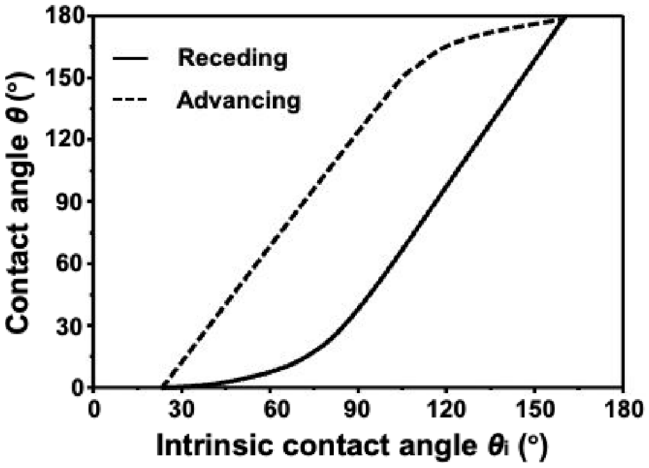

Figure 8. θ_r and θ_a as a function of θ_i [from Valvatne and Blunt (ref 56), based on Morrow (ref 60)]. (Adapted with permission from ref 56. Copyright 2004 American Geophysical Union. Adapted with permission from ref 60, Copyright 1975 Petroleum Society of Canada.)

In this work, we discuss the effect of gas trapping on hysteresis in P_c and k_r in dissociating HBS, namely, pore structure and wettability. We used the correlation proposed by Morrow;[60] the intrinsic contact angles θ_i, θ_r, and θ_a values are defined as shown in Figure 8. During the drying cycle, θ_r was set to 0° everywhere. During the wetting cycle, we adjusted θ_i in the range of 30−50° and 130−150° to obtain a water-wet system or gas-wet system, respectively. We assumed that the setting of the hydrate contact angle follows that of the sand. Here, the effect of hydrate phase transition on contact angle was not considered.[61,62]

2.7. Water and Gas Flow Simulation Conditions. In this study, an initially water-saturated network model was displaced by gas to connate water saturation. In HBS, we assumed that water could remain connected when the effective water saturation, S_{we}, decreased from 1.00 to 0.00; genuinely irreducible saturation was not allowed from clays or disconnected water, as explained by Zhao et al.[63] The detailed fluid characteristics and simulation conditions are summarized in Table 1.

Table 1. Fluid and Sediment Characteristics Used in the Simulation for Dissociating HBS

parameter	value
surface tension, σ (N/m)[a]	72×10^{-3}
water viscosity, μ_w (Pa·s)	1.05×10^{-3}
gas viscosity, μ_g (Pa·s)	1.10×10^{-5}
water density, ρ_w (kg/m^3)	998.83
gas density,ρ_g (kg/m^3)	4.02

[a]σ refers to laboratory tests by Yasuda et al. (ref 64).

3. RESULTS AND DISCUSSION

3.1. Pore Network Properties in Dissociating HBS. In this study, hydrates in the pore space have cementing and grain-coating pore habits. As a hydrate dissociation process, secondary hydrate formation was observed (Figure 2b). Secondary hydrate formation has at least two sources: local low temperature and local repressurization. The endothermic reaction of hydrate dissociation, compounded by the Joule−Thomson effect, causes the local low temperature in the specimen.[65] Local repressurization originates from P_c[66] and local plugging of fluid flow channels.[67] Secondary hydrate formation mainly developed on the existing hydrate shell surfaces, which had complete or semicomplete host structures, and this feature facilitated the secondary formation of the hydrate.[48] Moreover, hydrate dissociation provides free water in the gas-saturation pore space, and hydrate shell surfaces are rich in host-guest molecules, which further promotes the secondary hydrate formation.[48]

Parts a−c of Figure 9 show that the pore size R_p, throat size R_t, and n distribution move left and become smaller when S_h increases from 0.37 to 0.53. In addition, G_p, G_t, and the r_p distributions showed a small variation (Figure 9, parts d and e), where r_p is the ratio of R_p to the linked average R_t. These results reveal that the connectivity of pores and throats decreases because secondary hydrate formation blocks the pore space and decreases the number and size of the pores and throats. At the end of dissociation, the hydrates are completely dissociated, and a larger pore space occurs in the specimen. Therefore, the number and size of the balls and sticks increase when S_h decreases from 0.53 to 0.00. As dissociation proceeds further, the R_p, R_t, and n distribution curves move right and become larger. This is because dissociated hydrates result in more pore space, and thus the specimen will have a well-connected pore space. Moreover, the G_p and G_p distributions move left and become smaller. The r_p distribution moves to the right and becomes larger. In principle, well-connected hydrate-free specimens are more likely to have a higher G and lower r_p. Therefore, there is no direct relationship between S_h, G, and r_p.

3.2. Trapping in Dissociating HBS. Trapping occurs in the drying and wetting cycles surrounded by the invading fluid.[56] In this section, we analyzed only the wetting trapping (gas trapping) in dissociating HBS. This is because drying trapping (water trapping) has little effect on global water connectivity, as connate water usually exists in the grooves, crevices, and corners, or as a thin layer on the rock surface, which ensures global water connectivity.[56] Therefore, we investigated how different wettability options (water-wet or gas-wet) and changes in pore structure affected the gas trapping of dissociating HBS.

Comparison of the water-wet and gas-wet systems showed that the variations of S_{ger} were extremely sensitive (Figure 10). S_{ger} in a gas-wet system was lower than that in a water-wet system, as shown in Figure 10. This is because no snap-off exists in the gas-wet system. A comparison of S_{ger} trends between the water-wet and gas-wet systems demonstrates a similar behavior during the hydrate dissociation process.

Figure 10 also shows that S_{ger} increases when S_h increases from 0.37 to 0.53. As hydrate dissociation proceeds, S_{ger} decreases as S_h decreases from 0.53 to 0.00. These results indicate that hydrate dissociation affects gas trapping in dissociating HBS. To illustrate the competition between piston-like displacement, pore body filling, snap-off, and

https://doi.org/10.1021/acs.energyfuels.2c01306
Energy Fuels 2022, 36, 10572−10582

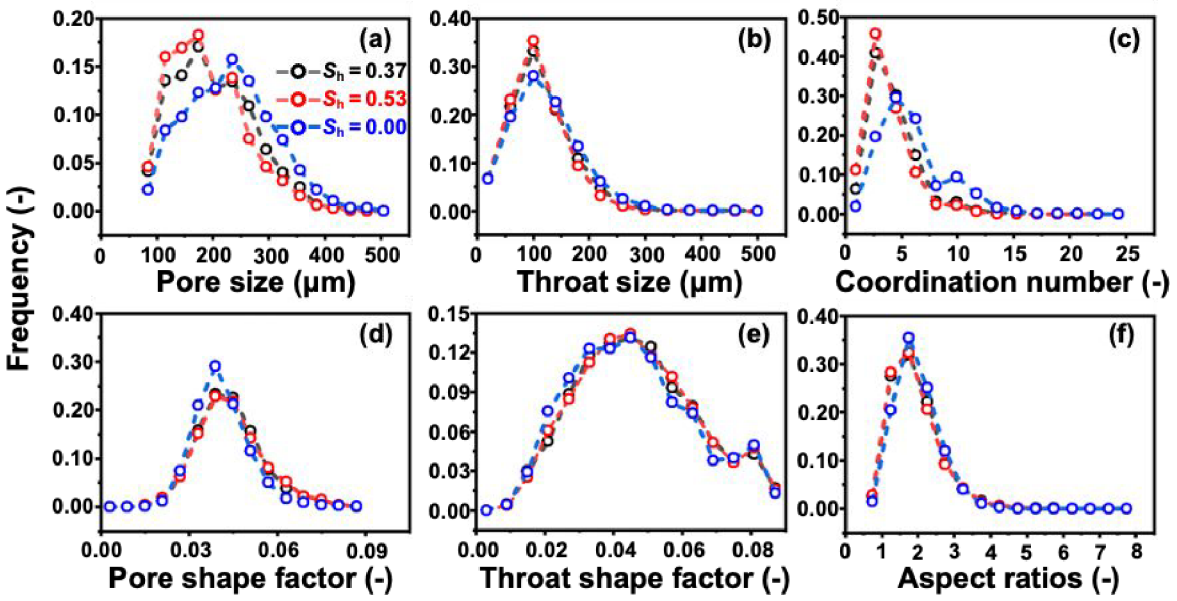

Figure 9. Variation of the pore structure in dissociating HBS: (a) R_p, (b) R_t, (c) n, (d) G_p, (e) G_t, and (f) r_p.

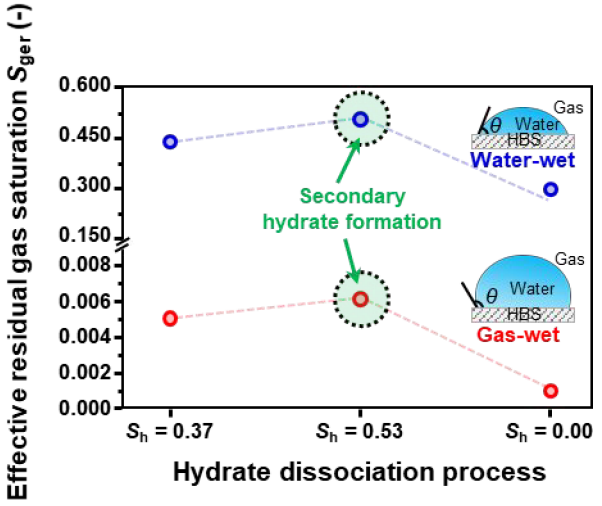

Figure 10. Variations of S_{ger} in dissociating HBS; the blue and red lines represent the water-wet and gas-wet systems, respectively.

uninvaded pores and throats in the pore space, we quantified the frequency of these flow patterns and uninvaded pores and throats using pore-scale modeling, as shown in Figure 11. The results reveal that the piston-like displacement is a dominant flow pattern in dissociating HBS. Secondary hydrate formation results in more smaller pore space and more gas trapping by water layers. Conversely, complete hydrate dissociation provides more pore space, which is beneficial for suppressing gas trapping.

3.3. Hysteresis in P_c in Dissociating HBS. Figure 12a shows the hysteresis variations of P_c in dissociating HBS in a water-wet system. Each plot shows that the wetting P_c curves are lower than the drying P_c curves at the same S_{we}. Three reasons account for the occurrence of hysteresis in P_c between drying and wetting: (i) trapping, (ii) different flow patterns (filling processes), and (iii) contact angle hysteresis.[43] Gas trapping in the pore space would shift the P_c curves during the wetting cycle. There is only a piston-like displacement during the drying cycle; however, an extra flow pattern of snap-off and pore body filling can occur during the wetting cycle. The threshold capillary pressure, P_c^t, for snap-off and pore body filling in the wetting cycle is lower than that of the piston-like displacement in the drying cycle with the same pore space. For more details on the P_c^t calculation, please refer to Appendix S1. The contact angle hysteresis θ_a in the wetting cycle is larger than θ_r in the drying cycle with the same pore space,[43] and then P_c^t for the wetting cycle is lower than P_c^t for drying cycle. Therefore, the wetting P_c curves are lower than the drying P_c curves at the same S_{we} at each hydrate dissociation stage.

Figure 12a also shows the variation of P_c during the hydrate dissociation process. There is a difference in the degree of hysteresis in P_c between the drying and wetting cycles. The secondary hydrate formation induced a greater degree of hysteresis. As S_h decreases from 0.53 to 0.00, hysteresis in P_c becomes insignificant.

In the gas-wet system, a similar hysteresis is also evident in the P_c behavior, as shown in Figure 12b. The wetting P_c curves are lower than the drying P_c curves at the same S_{we}. However, the P_c in the drying cycle can drop to zero, and further displacement occurs at a negative P_c ($P_c < 0$) in the gas-wet system. A negative P_c ($P_c < 0$) is caused by the large contact angle in the gas-wet system, which is difficult to measure experimentally. Figure 12b illustrates the effect of pore structure changes on hysteresis in P_c during the hydrate dissociation. Moreover, the degree of hysteresis in the P_c trends is similar to that in the water-wet system.

3.4. Hysteresis in k_r in Dissociating HBS. Figure 13a shows the hysteresis in k_r curves between the drying and wetting cycles in dissociating HBS for the water-wet system. As expected, each plot shows a small amount of hysteresis between the wetting k_{rw} curve and drying k_{rw} curve. The wetting k_{rg} curves are lower than the drying k_{rg} curves, at least at higher S_{we}. Water preferentially flows through the smallest regions of the pore space by snap-off and bypassing, rather than through larger pores.[58,68] Snap-off is favorable for gas trapping. The gas contained in the narrow throats is trapped and disconnected, which hinders gas flow pathways, at least at high S_{we}.[43,58] Hence, the wetting k_{rg} curves shift to a lower S_{we} (higher S_g), at least at high S_{we}, owing to gas trapping. This

https://doi.org/10.1021/acs.energyfuels.2c01306
Energy Fuels 2022, 36, 10572−10582

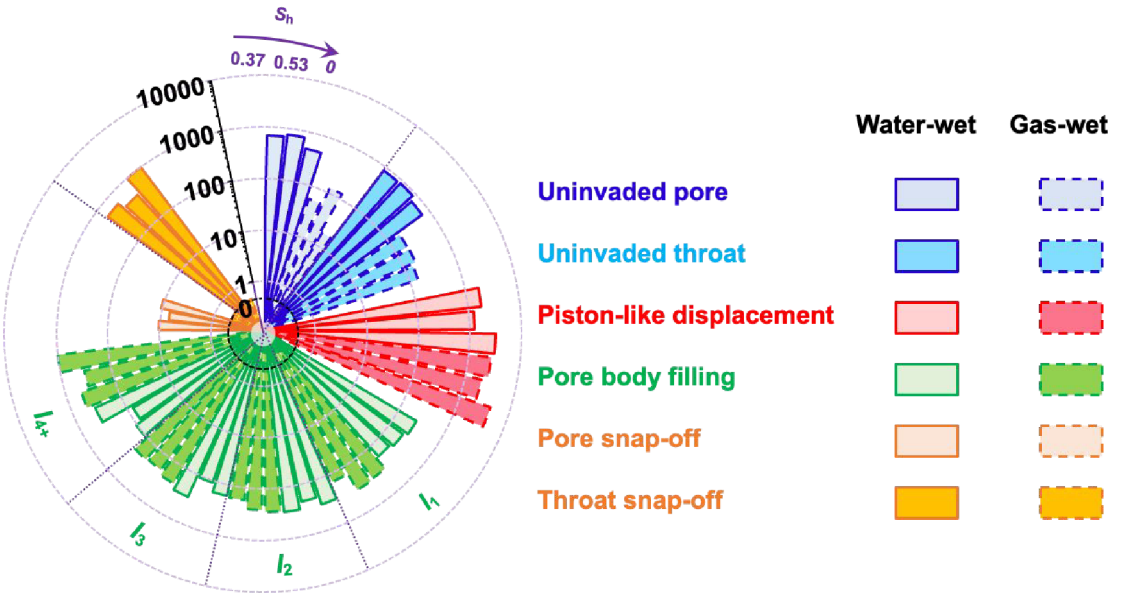

Figure 11. Flow pattern statistics for the wetting process in dissociating HBS.

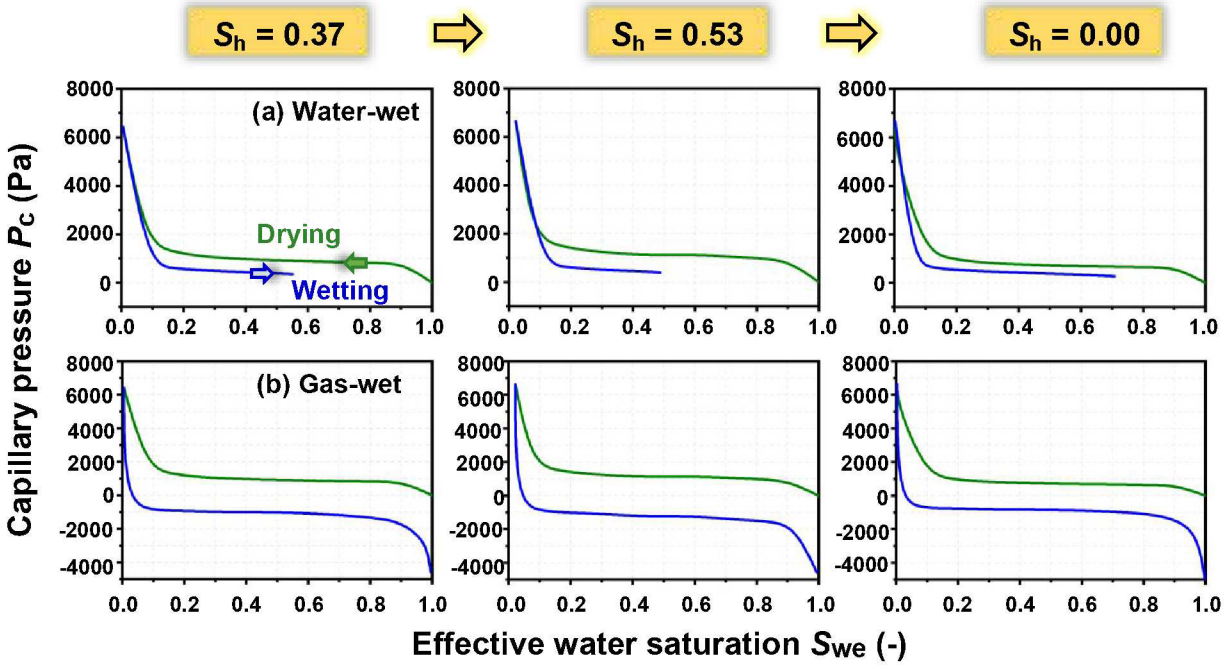

Figure 12. Variation of P_c between drying and wetting cycles in dissociating HBS: (a) water-wet system; (b) gas-wet system.

causes the wetting k_{rw} curves to be higher than the drying k_{rw} curves. However, the unmovable gas may hinder water flow and cause the wetting k_{rw} curves to be lower than the drying k_{rw} curves. Because there are two opposing effects on the wetting k_{rw} curves, there exists an extremely low hysteresis between the wetting and drying k_{rw} curves.[69]

Hydrate dissociation has less effect on the degree of hysteresis in k_{rw} in the water-wet system as shown in Figure 13a. As S_h increases from 0.37 to 0.53, the degree of hysteresis in k_{rg} between the drying and wetting cycles increases at high S_{we}. With further hydrate dissociation, the degree of hysteresis in k_{rg} becomes smaller at high S_{we}. The results indicate that the degree of hysteresis in k_{rg} is primarily controlled by the pore structure in water-wet dissociating HBS. Secondary hydrate formation clogs the pore space and causes more gas to be trapped in the narrow throats. As a result, the gas is disconnected, which hinders gas flow pathways at high S_{we}. Hence, secondary hydrate formation significantly suppressed the wetting k_{rg} curve at high S_{we}. On the contrary, hydrate dissociation caused more pore space to occur in the specimen (S_h = 0.00); small gas trapping is desirable for gas flow in pore spaces.

Figure 13b shows that the wetting k_{rw} curves are higher than the drying k_{rw} curves, and the wetting k_{rg} curves are lower than those in the gas-wet system. Water invades and occupies the center of large pore spaces, and as such this may cause the wetting k_{rw} curve to be higher than the drying k_{rw} curve.[70] Thus, the wetting k_{rg} curve is lower than the drying k_{rg} curve.

https://doi.org/10.1021/acs.energyfuels.2c01306
Energy Fuels 2022, 36, 10572−10582

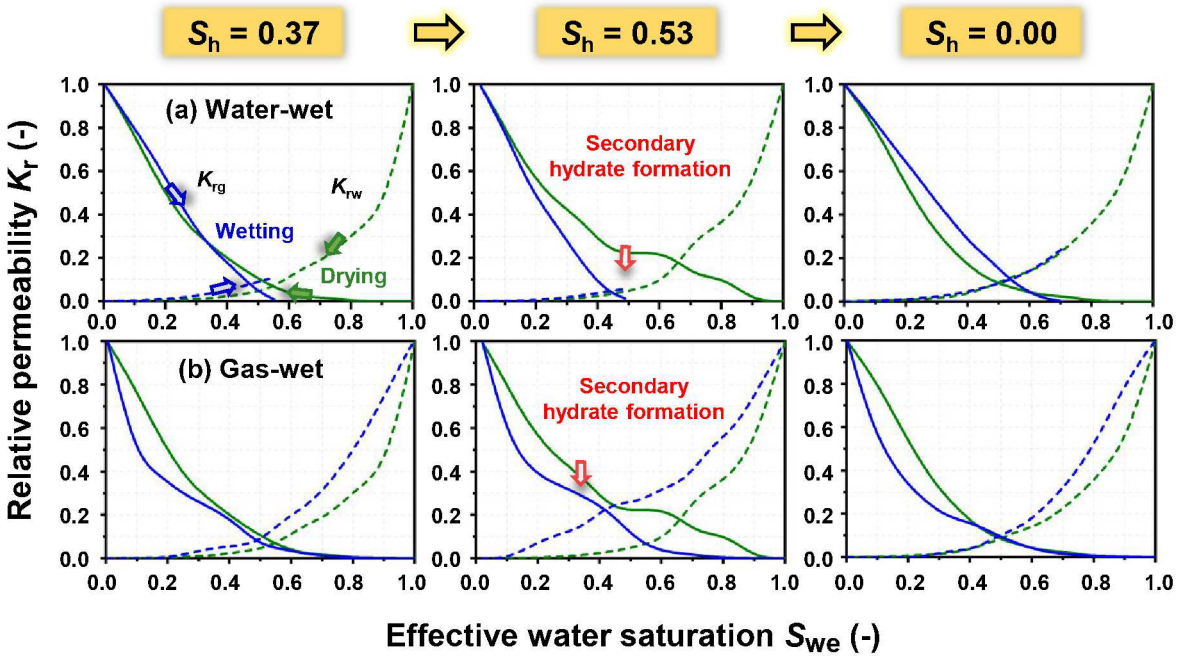

Figure 13. k_r variation with S_{we} during the drying and wetting cycles in dissociating HBS: (a) water-wet system; (b) gas-wet system.

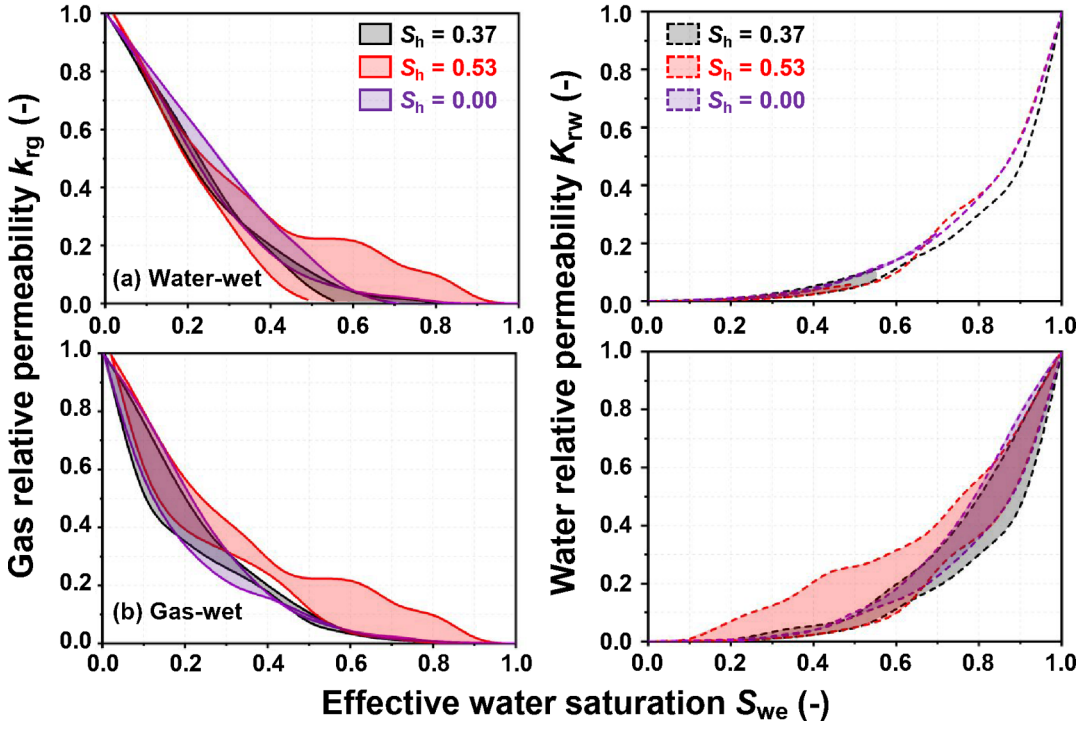

Figure 14. Dynamic scanning flow between the drying and wetting cycles in dissociating HBS: (a) water-wet system; (b) gas-wet system.

Figure 13b illustrates the degree of hysteresis in k_{rw} and k_{rg} between the drying and wetting cycles in the gas-wet system. At the beginning of hydrate dissociation, the degree of hysteresis in k_{rw} and k_{rg} increases. With further hydrate dissociation, the degree of hysteresis in k_{rw} and k_{rg} decreases as S_h decreases from 0.53 to 0.00. We inferred that secondary hydrate formation provided more smaller space, which may also contribute to the connectivity of the water that is occupying the center of adjacent pore spaces. This may also be an important factor in increasing the degree of hysteresis in k_r during the secondary hydrate formation.

The water and gas displacement sequences are complex in dissociating HBS, involving hydrate dissociation, secondary hydrate formation,[47] and fluid (e.g., hot water) injection.[38] Consequently, drying and wetting cycles may occur simultaneously in dissociating HBS. Our study proposes the use of dynamic scanning flow to analyze the flow of water and gas in dissociating HBS.

https://doi.org/10.1021/acs.energyfuels.2c01306
Energy Fuels 2022, 36, 10572−10582

Figure 14a presents the dynamic scanning flow in the water-wet system. The k_{rg} and k_{rw} scanning regions shifted down as S_h increased from 0.37 to 0.53 at low S_{we}, and subsequently, these scanning regions shifted up at the end of hydrate dissociation (S_h = 0.00). Therefore, secondary hydrate formation clogs the pore space, trapping more gas, and hinders gas and water flow pathways, and gas flowability improves in the hydrate-free specimen.[71] Figure 14b demonstrates the dynamic scanning flow in the gas-wet system. However, these scanning regions are more complicated than those in water-wet systems.

4. CONCLUSIONS

We combined *in situ* microfocus X-ray CT and PNM simulation to analyze how the wettability (water-wet or gas-wet) and pore structure changes during hydrate dissociation influence gas trapping and hysteresis in P_c and k_r. On the basis of this study, the following conclusions are drawn:

(1) Hydrate dissociation has a significant impact on gas trapping. Secondary hydrate formation causes a large number of uninvaded pores and throats, resulting in S_{gr} increases.

(2) Secondary hydrate formation increases the degree of hysteresis in P_c between the drying and wetting cycles. The wetting P_c curves are lower than the drying P_c curves at the same S_{we} in dissociating HBS. Different k_r curve trends from both water and gas are explained by different water and gas flow scenarios in dissociating HBS.

(3) We also propose to use dynamic scanning flow for analyzing complex water and gas displacement sequences in dissociating HBS. The wettability has a strong impact on the dynamic scanning flow for k_{rg} and k_{rw}. In the water-wet system, secondary hydrate formation causes the k_{rg} and k_{rw} scanning regions to shift down. There is more complexity in the gas-wet system. It is challenging to predict the dynamic k_{rg} and k_{rw} scanning flow in dissociating HBS.

This fundamental information suggests considering wettability alteration and gas trapping in the P_c and k_r hysteresis for accurately predicting water and gas in HBS, to further improve understanding of the process of HBS exploitation at the pore scale.

■ ASSOCIATED CONTENT

Supporting Information

The Supporting Information is available free of charge at https://pubs.acs.org/doi/10.1021/acs.energyfuels.2c01306.

Relative permeability and capillary pressure calculation methods and hydrate saturation, water saturation, gas saturation, effective water saturation, and gas saturation definitions (PDF)

■ AUTHOR INFORMATION

Corresponding Authors

Aliakbar Hassanpouryouzband − *School of Geosciences, University of Edinburgh, Grant Institute, Edinburgh EH9 3FE, U.K.;* orcid.org/0000-0003-4183-336X; Email: Hssnpr@ed.ac.uk

Lunxiang Zhang − *Key Laboratory of Ocean Energy Utilization and Energy Conservation of the Ministry of Education, Dalian University of Technology, Dalian 116024, China;* orcid.org/0000-0002-3959-7575; Email: lunxiangzhang@dlut.edu.cn

Authors

Min Li − *Key Laboratory of Ocean Energy Utilization and Energy Conservation of the Ministry of Education, Dalian University of Technology, Dalian 116024, China*

Zhenhe Jian − *Key Laboratory of Ocean Energy Utilization and Energy Conservation of the Ministry of Education, Dalian University of Technology, Dalian 116024, China*

Complete contact information is available at: https://pubs.acs.org/10.1021/acs.energyfuels.2c01306

Author Contributions

M.L. was responsible for conceptualization, methodology, investigation, and writing the original draft; Z.J. was responsible for investigation; A.H. was responsible for supervision, writing, reviewing, editing, and resources; L.Z. was responsible for methodology, supervision, writing, reviewing, editing, and resources.

Notes

The authors declare no competing financial interest.

■ ACKNOWLEDGMENTS

We thank Peng Wu for sharing his experimental data. The authors of this work express their appreciation to the National Natural Science Foundation of China (Grant Nos. 52006024 and U21B2065).

■ ABBREVIATIONS

3D, three-dimensional; CT, computed tomography; HBS, hydrate-bearing sediments; PNM, pore network model

■ NOMENCLATURE

A = area, m^2
G = shape factor, -
k_{int} = intrinsic permeability, m^2
k_{eff} = effective permeability, m^2
k_r = relative permeability, -
n = coordination number, -
P_c = capillary pressure, Pa
P_c^t = threshold capillary pressure, Pa
R = radius, m
V = volume, m^3
S = saturation, -
S_{we} = effective water saturation, -
S_{ge} = effective gas saturation, -
σ = surface tension, N/m
θ_i = intrinsic contact angle, deg
θ_a = advancing contact angle, deg
θ_r = receding contact angle, deg
μ = viscosity, Pa·s
P = density, kg/m^3
ϕ = porosity, -

■ SUBSCRIPTS

h, hydrate; w, water; g, gas; p, pore; t, throat; ger, effective residual gas

REFERENCES

(1) Ripmeester, J. A.; Alavi, S. An Introduction to Clathrate Hydrates. In *Clathrate Hydrates*; Ripmeester, J. A., Alavi, S., Eds.; Wiley, 2022.

(2) Linga, P.; Kumar, R.; Lee, J. D.; Ripmeester, J.; Englezos, P. A new apparatus to enhance the rate of gas hydrate formation: Application to capture of carbon dioxide. *Int. J. Greenh. Gas Control* **2010**, *4* (4), 630−637.

(3) Kvenvolden, K. A.; Lorenson, T. D. The Global Occurrence of Natural Gas Hydrate. In *Natural Gas Hydrates: Occurrence, Distribution, and Detection*; Paull, C. K., Dillon, W. P., Eds.; Geophysical Monograph Series *124*; American Geophysical Union: Washington, DC, 2001.

(4) Hassanpouryouzband, A.; Joonaki, E.; Vasheghani Farahani, M.; Takeya, S.; Ruppel, C.; Yang, J.; English, N. J.; Schicks, J. M.; Edlmann, K.; Mehrabian, H.; Aman, Z. M.; Tohidi, B. Gas hydrates in sustainable chemistry. *Chem. Soc. Rev.* **2020**, *49* (15), 5225−5309.

(5) Zhao, J.; Zhu, Z.; Song, Y.; Liu, W.; Zhang, Y.; Wang, D. Analyzing the process of gas production for natural gas hydrate using depressurization. *Appl. Energy* **2015**, *142*, 125−134.

(6) Jaiswal, N. J. *Measurement of Gas-Water Relative Permeabilities in Hydrate Systems*. M.S. Thesis, University of Alaska, Fairbanks, AK, 2004.

(7) Zhang, L.; Dong, H.; Dai, S.; Kuang, Y.; Yang, L.; Wang, J.; Zhao, J.; Song, Y. Effects of depressurization on gas production and water performance from excess-gas and excess-water methane hydrate accumulations. *Chem. Eng. Journal* **2022**, *431*, 133223.

(8) Kneafsey, T. J.; Seol, Y.; Gupta, A.; Tomutsa, L. Permeability of Laboratory-Formed Methane-Hydrate-Bearing Sand: Measurements and Observations Using X-Ray Computed Tomography. *Spe J.* **2011**, *16* (1), 78−94.

(9) Zhang, L.; Ge, K.; Wang, J.; Zhao, J.; Song, Y. Pore-scale investigation of permeability evolution during hydrate formation using a pore network model based on X-ray CT. *Mar. Pet. Geol* **2020**, *113*, 104157.

(10) Chuvilin, E.; Grebenkin, S.; Zhmaev, M. Gas Permeability of Sandy Sediments: Effects of Phase Changes in Pore Ice and Gas Hydrates. *Energy Fuels* **2021**, *35* (9), 7874−7882.

(11) Li, G.; Zhan, L.; Yun, T.; Dai, S. Pore-Scale Controls on the Gas and Water Transport in Hydrate-Bearing Sediments. *Geophys. Res. Lett.* **2020**, *47* (12), e2020GL086990.

(12) Zhang, J.; Liu, X.; Chen, D.; Yin, Z. An investigation on the permeability of hydrate-bearing sediments based on pore-scale CFD simulation. *Int. J. Heat Mass Transf* **2022**, *192*, 122901.

(13) Thatcher, K. E.; Westbrook, G. K.; Sarkar, S.; Minshull, T. A. Methane release from warming-induced hydrate dissociation in the West Svalbard continental margin: Timing, rates, and geological controls. *J. Geophys.l Res.: Solid Earth* **2013**, *118* (1), 22−38.

(14) Choi, J.-H.; Myshakin, E. M.; Lei, L.; Kneafsey, T. J.; Seol, Y. An experimental system and procedure of unsteady-state relative permeability test for gas hydrate-bearing sediments. *J. Nat. Gas Sci. Eng.* **2020**, *83*, 103545.

(15) Sun, H.; Chen, B.; Pang, W.; Song, Y.; Yang, M. Investigation on plugging prediction of multiphase flow in natural gas hydrate sediment with different field scales. *Fuel* **2022**, *325*, 124936.

(16) Wang, J.; Zhao, J.; Zhang, Y.; Wang, D.; Li, Y.; Song, Y. Analysis of the influence of wettability on permeability in hydrate-bearing porous media using pore network models combined with computed tomography. *J. Nat. Gas Sci. Eng.* **2015**, *26*, 1372−1379.

(17) Fan, M.; McClure, J. E.; Armstrong, R. T.; Shabaninejad, M.; Dalton, L. E.; Crandall, D.; Chen, C. Influence of Clay Wettability Alteration on Relative Permeability. *Geophys. Res. Lett.* **2020**, *47* (18), e2020GL088545.

(18) Delli, M. L.; Grozic, J. L. H. Experimental determination of permeability of porous media in the presence of gas hydrates. *J. Pet. Sci. Eng.* **2014**, *120*, 1−9.

(19) Kumar, A.; Maini, B.; Bishnoi, P. R.; Clarke, M.; Zatsepina, O.; Srinivasan, S. Experimental determination of permeability in the presence of hydrates and its effect on the dissociation characteristics of gas hydrates in porous media. *J. Pet. Sci. Eng.* **2010**, *70* (1−2), 114−122.

(20) Yoneda, J.; Oshima, M.; Kida, M.; Kato, A.; Konno, Y.; Jin, Y.; Jang, J.; Waite, W. F.; Kumar, P.; Tenma, N. Permeability variation and anisotropy of gas hydrate-bearing pressure-core sediments recovered from the Krishna−Godavari Basin, offshore India. *Mar. Pet. Geol* **2019**, *108*, 524−536.

(21) Konno, Y.; Yoneda, J.; Egawa, K.; Ito, T.; Jin, Y.; Kida, M.; Suzuki, K.; Fujii, T.; Nagao, J. Permeability of sediment cores from methane hydrate deposit in the Eastern Nankai Trough. *Mar. Pet. Geo* **2015**, *66*, 487−495.

(22) Fujii, T.; Suzuki, K.; Takayama, T.; Tamaki, M.; Komatsu, Y.; Konno, Y.; Yoneda, J.; Yamamoto, K.; Nagao, J. Geological setting and characterization of a methane hydrate reservoir distributed at the first offshore production test site on the Daini-Atsumi Knoll in the eastern Nankai Trough, Japan. *Mar. Pet. Geo* **2015**, *66*, 310−322.

(23) Johnson, A.; Patil, S.; Dandekar, A. Experimental investigation of gas-water relative permeability for gas-hydrate-bearing sediments from the Mount Elbert Gas Hydrate Stratigraphic Test Well, Alaska North Slope. *Mar. Pet. Geo* **2011**, *28* (2), 419−426.

(24) Masuda, Y.; Naganawa, S. Numerical Calculation of Gas-Production Performance from Reservoirs Containing Natural Gas Hydrates. *Proceedings of the Western Regional Meeting of the Society of Petroleum Engineers*, Long Beach, CA, June 25−27, 1997.

(25) Kleinberg, R. L.; Flaum, C.; Griffin, D. D.; Brewer, P. G.; Malby, G. E.; Peltzer, E. T.; Yesinowski, J. P. Deep sea NMR: Methane hydrate growth habit in porous media and its relationship to hydraulic permeability, deposit accumulation, and submarine slope stability. *J. Geophys. Res.* **2003**, *108* (B10), 2508.

(26) Hou, J.; Ji, Y.; Zhou, K.; Liu, Y.; Wei, B. Effect of hydrate on permeability in porous media: Pore-scale micro-simulation. *Int. J. Heat Mass Transf* **2018**, *126*, 416−424.

(27) Wang, J.-Q.; Zhao, J.-F.; Yang, M.-J.; Li, Y.-H.; Liu, W.-G.; Song, Y.-C. Permeability of laboratory-formed porous media containing methane hydrate: Observations using X-ray computed tomography and simulations with pore network models. *Fuel* **2015**, *145*, 170−179.

(28) Blunt, M. J.; Bijeljic, B.; Dong, H.; Gharbi, O.; Iglauer, S.; Mostaghimi, P.; Paluszny, A.; Pentland, C. Pore-scale imaging and modelling. *Adv. Water Resour* **2013**, *51*, 197−216.

(29) Cnudde, V.; Boone, M. N. High-resolution X-ray computed tomography in geosciences: A review of the current technology and applications. *Earth-Science Reviews* **2013**, *123*, 1−17.

(30) Wildenschild, D.; Sheppard, A. P. X-ray imaging and analysis techniques for quantifying pore-scale structure and processes in subsurface porous medium systems. *Adv. Water Resour* **2013**, *51*, 217−246.

(31) Dong, H.; Blunt, M. J. Pore-network extraction from micro-computerized-tomography images. *Phys. Rev. E* **2009**, *80* (3), 036307.

(32) Yang, X.; Mehmani, Y.; Perkins, W. A.; Pasquali, A.; Schönherr, M.; Kim, K.; Perego, M.; Parks, M. L.; Trask, N.; Balhoff, M. T.; Richmond, M. C.; Geier, M.; Krafczyk, M.; Luo, L.-S.; Tartakovsky, A. M.; Scheibe, T. D. Intercomparison of 3D pore-scale flow and solute transport simulation methods. *Adv. Water Resour* **2016**, *95*, 176−189.

(33) Raeini, A. Q.; Bijeljic, B.; Blunt, M. J. Generalized network modeling: Network extraction as a coarse-scale discretization of the void space of porous media. *Phys. Rev. E* **2017**, *96* (1−1), 013312.

(34) Rasmusson, K.; Rasmusson, M.; Tsang, Y.; Benson, S.; Hingerl, F.; Fagerlund, F.; Niemi, A. Residual trapping of carbon dioxide during geological storage—Insight gained through a pore-network modeling approach. *Int. J. Greenhouse Gas Control* **2018**, *74*, 62−78.

(35) Arshadi, M.; Gesho, M.; Qin, T.; Goual, L.; Piri, M. Impact of mineralogy and wettability on pore-scale displacement of NAPLs in heterogeneous porous media. *J. Contam Hydrol* **2020**, *230*, 103599.

(36) Singh, K.; Bultreys, T.; Raeini, A. Q.; Shams, M.; Blunt, M. J. Imbibition in porous media: correlations of displacement events with pore-throat geometry and the identification of a new type of pore snap-off. *EarthArXiv*, August 8, **2019**. DOI: 10.31223/osf.io/62gfr.

https://doi.org/10.1021/acs.energyfuels.2c01306
Energy Fuels 2022, 36, 10572−10582

(37) Mahabadi, N.; Dai, S.; Seol, Y.; Sup Yun, T.; Jang, J. The water retention curve and relative permeability for gas production from hydrate-bearing sediments: pore-network model simulation. *Geochem., Geophys., Geosyst* **2016**, *17* (8), 3099−3110.
(38) Wang, J.; Zhang, L.; Zhao, J.; Ai, L.; Yang, L. Variations in permeability along with interfacial tension in hydrate-bearing porous media. *J. Nat. Gas Sci. Eng.* **2018**, *51*, 141−146.
(39) JERAULD, G. R.; SALTER, S. J. The effect of pore-structure on hysteresis in relative permeability and capillary pressure: pore-level modeling. *Transp. Porous Media* **1990**, *5*, 103−151.
(40) Dixit, A. B.; McDougall, S. R.; Sorbie, K. S. A Pore-Level Investigation of Relative Permeability Hysteresis in Water-Wet System. *SPE J.* **1998**, *3* (02), 115−123.
(41) Dernaika, M. R.; Basioni, M. A.; Dawoud, A.; Kalam, M. Z.; Skjaeveland, S. M. Variations in bounding and scanning relative permeability curves with different carbonate rock type. *SPE Reservoir Eval. Eng.* **2013**, *16* (03), 265−280.
(42) Meisenheimer, D. E.; McClure, J. E.; Rivers, M. L.; Wildenschild, D. Exploring the effect of flow condition on the constitutive relationships for two-phase flow. *Adv. Water Resour* **2020**, *137*, 103506.
(43) Blunt, M. J. *Multiphase Flow in Permeable Media*; Cambridge University Press: Cambridge, U.K., 2017.
(44) Braun, E. M.; Holland, R. F. Relative Permeability Hysteresis: Laboratory Measurements and a Conceptual Model. *SPE Reservoir Eng.* **1995**, *10* (03), 222−228.
(45) Plohr, B.; Marchesin, D.; Bedrikovetsky, P.; Krause, P. Modeling hysteresis in porous media flow via relaxation. *Computational Geosciences* **2001**, *5*, 225−256.
(46) Konno, Y.; Masuda, Y.; Takenaka, T.; Oyama, H.; Ouchi, H.; Kurihara, M. Numerical Study on Permeability Hysteresis during Hydrate Dissociation in Hot Water Injection. *Proceedings of the 6th International Conference on Gas Hydrates (ICGH 2008)*, Vancouver, BC, Canada, July 6−10, 2008.
(47) Moridis, G. J.; Collett, T. S.; Pooladi-Darvish, M.; Hancock, S.; Santamarina, C.; Boswell, R.; Kneafsey, T.; Rutqvist, J.; Kowalsky, M. B.; Reagan, M. T.; Sloan, E. D.; Sum, A. K.; Koh, C. A. Challenges, Uncertainties, and Issues Facing Gas Production From Gas-Hydrate Deposits. *SPE Reservoir Eval. Eng.* **2011**, *14* (01), 76−112.
(48) Wu, P.; Li, Y.; Sun, X.; Liu, W.; Song, Y. Microstructure evolution of hydrate-bearing sands during thermal dissociation and ensued impacts on the mechanical and seepage characteristics. *J. Geophys. Res.: Solid Earth* **2020**, *125* (12), e2019JB019103.
(49) Li, M.; Wu, P.; Zhou, S.; Zhang, L.; Yang, L.; Li, Y.; Liu, Y.; Zhao, J.; Song, Y. Permeability Analysis of Hydrate-Bearing Sediments during the Hydrate Formation Process. *Energy Fuels* **2021**, *35*, 19606.
(50) Chaouachi, M.; Falenty, A.; Sell, K.; Enzmann, F.; Kersten, M.; Haberthür, D.; Kuhs, W. F. Microstructural evolution of gas hydrates in sedimentary matrices observed with synchrotron X-ray computed tomographic microscopy. *Geochem., Geophys., Geosyst* **2015**, *16* (6), 1711−1722.
(51) Hyodo, M.; Li, Y.; Yoneda, J.; Nakata, Y.; Yoshimoto, N.; Nishimura, A.; Song, Y. Mechanical behavior of gas-saturated methane hydrate-bearing sediments. *J. Geophys.l Res.: Solid Earth* **2013**, *118* (10), 5185−5194.
(52) Hyodo, M.; Yoneda, J.; Yoshimoto, N.; Nakata, Y. Mechanical and dissociation properties of methane hydrate-bearing sand in deep seabed. *Soils and Foundations* **2013**, *53* (2), 299−314.
(53) Bachmat, Y.; Bear, J. On the Concept and Size of a Representative Elementary Volume (REV). In *Advances in Transport Phenomena in Porous Media*; Bear, J., Corapcioglu, M. Y., Eds.; NATO ASI Series *128*; Springer: Dordrecht, Netherlands, 1987.
(54) Lie, K.-A.; Mallison, B. T. Mathematical Models for Oil Reservoir Simulation. In *Encyclopedia of Applied and Computational Mathematics*; Engquist, B., Ed.; Springer Verlag: Berlin Heidelberg, Germany, 2015.
(55) Bultreys, T.; Lin, Q.; Gao, Y.; Raeini, A. Q.; AlRatrout, A.; Bijeljic, B.; Blunt, M. J. Validation of model predictions of pore-scale fluid distributions during two-phase flow. *Physical review. E* **2018**, *97* (5−1), 053104.
(56) Valvatne, P. H.; Blunt, M. J. Predictive pore-scale modeling of two-phase flow in mixed wet media. *Water Resour. Res.* **2004**, *40* (7), W07406.
(57) Singh, K.; Menke, H.; Andrew, M.; Lin, Q.; Rau, C.; Blunt, M. J.; Bijeljic, B. Dynamics of snap-off and pore-filling events during two-phase fluid flow in permeable media. *Sci. Rep.* **2017**, *7* (1), 5192.
(58) Spiteri, E. J.; Juanes, R.; Blunt, M. J.; Orr, F. M. A New Model of Trapping and Relative Permeability Hysteresis for All Wettability Characteristics. *SPE J.* **2008**, *13* (03), 277−288.
(59) Sedaghatinasab, R.; Kord, S.; Moghadasi, J.; Soleymanzadeh, A. Relative Permeability Hysteresis and Capillary Trapping during CO2 EOR and Sequestration. *Int.l J. Greenhouse Gas Control* **2021**, *106*, 103262.
(60) Morrow, N. R. Effects of surface roughness on contact angle with special reference to petroleum recovery. *J. Can. Pet. Technol.* **1975**, *14*, PETSOC-75-04-04.
(61) Stoner, H. M.; Phan, A.; Striolo, A.; Koh, C. A. Water Wettability Coupled with Film Growth on Realistic Cyclopentane Hydrate Surfaces. *Langmuir* **2021**, *37* (42), 12447−12456.
(62) Phan, A.; Stoner, H. M.; Stamatakis, M.; Koh, C. A.; Striolo, A. Surface morphology effects on clathrate hydrate wettability. *J. Colloid Interface Sci.* **2022**, *611*, 421−431.
(63) Zhao, X.; Blunt, M. J.; Yao, J. Pore-scale modeling: Effects of wettability on waterflood oil recovery. *J. Pet. Sci. Eng.* **2010**, *71* (3−4), 169−178.
(64) Yasuda, K.; Mori, Y. H.; Ohmura, R. Interfacial tension measurements in water−methane system at temperatures from 278.15 to 298.15 K and pressures up to 10 MPa. *Fluid Phase Equilib.* **2016**, *413*, 170−175.
(65) Seol, Y.; Myshakin, E. Experimental and Numerical Observations of Hydrate Reformation during Depressurization in a Core-Scale Reactor. *Energy Fuels* **2011**, *25* (3), 1099−1110.
(66) Henry, P.; Thomas, M.; Clennell, M. B. Formation of natural gas hydrates in marine sediments: 2. Thermodynamic calculations of stability conditions in porous sediments. *J. Geophys. Res.: Solid Earth* **1999**, *104* (B10), 23005−23022.
(67) Lee, J.; Park, S.; Sung, W. An experimental study on the productivity of dissociated gas from gas hydrate by depressurization scheme. *Energy Conversion and Management* **2010**, *51* (12), 2510−2515.
(68) Blunt, M. J.; Scher, H. Pore-level modeling of wetting. *Phys. Rev. E* **1995**, *52* (6), 6387−6403.
(69) Masalmeh, S. K. Experimental Measurements of Capillary Pressure and Relative Permeability Hysteresis. Presented at the SCA 2001 Conference, 2001; SCA 2001-23.
(70) Dernaika, M. R.; Kalam, M. Z.; Basioni, M.; Dawoud, A.; Skjæveland, S. M. Hysteresis of Capillary Pressure, Resistivity Index and Relative Permeability in Carbonate Rock Types. *Petrophysics* **2012**, *53* (05), 316−332.
(71) Li, M.; Zhou, S.; Wu, P.; Zhang, L.; Yang, L.; Li, Y.; Liu, Y.; Zhao, J.; Song, Y. Permeability analysis of hydrate-bearing sediments considering the effect of phase transition during the hydrate dissociation process. *J. Nat. Gas Sci. Eng.* **2022**, *97*, 104337.